crystals

MDPI

Article

Mechanical and Surface Characterization of Stainless-Steel Nitride Thin Films Deposited at Different Substrate Temperatures

Faisal Alresheedi

Department of Physics, College of Science, Qassim University, Buraidah 51452, Saudi Arabia; f.alresheedi@qu.edu.sa

Abstract

Stainless-steel nitride thin films were deposited onto silicon substrates at different temperatures ranging from 150 to 600 °C using reactive magnetron sputtering. The influence of substrate temperature on nitrogen incorporation, surface roughness, microstructure, and mechanical properties was systematically investigated. X-ray photoelectron spectroscopy (XPS) analysis showed that the nitrogen content increased with substrate temperature, reaching a maximum value of 34 wt.% at 350 °C, while at higher substrate temperatures (450–600 °C), the nitrogen content decreased. X-ray diffraction analysis revealed that the coating structure strongly depends on the substrate temperature. At temperatures above 450 °C, the films comprise a multiphase structure consisting of CrN, bcc-Fe, and Ni. In contrast, films deposited below 450 °C are dominated by the S-phase, corresponding to a nitrogen-supersaturated fcc structure. Scanning electron microscopy (SEM) analyses confirmed microstructural evolution with substrate temperature, showing fine, compact grains at lower temperatures and coarser structures at higher temperatures. Surface roughness measured by a profilometer exhibited a minimum at 350 °C. The mechanical performance of the films was evaluated using micro-Knoop hardness measurements, together with the calculated elastic strain indicator (H/E) and resistance to the plastic deformation parameter (H^3/E^2). The results showed that hardness and these mechanical indicators reached their maximum values at a substrate temperature of 350 °C. These findings provide valuable insight into the deposition–structure–property relationships of stainless-steel nitride thin films for wear-resistant and protective coating applications.

Keywords: thin films; stainless steel; crystal structure; mechanical properties; hardness

1. Introduction

Austenitic stainless steels such as AISI 304 and 316 are widely used due to their favorable combination of mechanical strength, toughness, and excellent corrosion resistance in a variety of harsh environments. Despite these advantages, their intrinsic wear resistance remains relatively low, which has driven extensive research into surface modification techniques aimed at enhancing hardness and reducing wear. One effective approach involves the incorporation of nitrogen into the surface region, either through implantation or diffusion, to form a hardened nitrogen-rich layer. Most conventional treatments rely on exposure to nitrogen-containing plasmas at elevated temperatures [1–8]. Nitrogen implantation has been achieved using low-energy, high-flux ion beams (0.7 keV) [1], as well as plasma immersion ion implantation techniques [2–4], where substrates are immersed in a plasma and subjected to high-voltage negative pulses. These treatments are typically carried out at substrate temperatures between 300 and 500 °C and have been shown to significantly enhance

Check for updates

Academic Editor: Dah-Shyang Tsai

Received: 15 January 2026
Revised: 28 January 2026
Accepted: 4 February 2026
Published: 6 February 2026

Copyright: © 2026 by the author. Licensee MDPI, Basel, Switzerland. This article is an open access article distributed under the terms and conditions of the Creative Commons Attribution (CC BY) license.

wear resistance compared to untreated stainless steel [8]. In addition to plasma-based treatments of bulk materials, significant attention has been directed toward the deposition of nitrogen-containing stainless-steel thin films using reactive magnetron sputtering [9–15]. For example, Saker et al. [9] reported the formation of nitrogen-supersaturated austenitic (fcc) films exhibiting high compressive residual stresses and improved hardness. Unlike plasma-treated bulk alloys, magnetron sputtering enables high nitrogen incorporation at substantially lower temperatures, even down to room temperature [15]. Moreover, stoichiometric metal nitride films with zinc-blende structures have been reported by Kapaganthu and Sun [11,12]. The crystal structures of nitrogen-modified stainless steels, whether produced by plasma treatments or thin-film deposition, have been extensively investigated, primarily using X-ray diffraction techniques. At substrate temperatures exceeding 500 °C, the formation of CrN is typically observed, whereas treatments below approximately 400 °C result in a nitrogen-supersaturated fcc phase. This metastable phase has been variously referred to as expanded austenite (EA) [16], γN [1,9], and S-phase [2,3,17,18], and is characterized by an exceptionally high interstitial nitrogen concentration, commonly in the range of 20–40 at.%. X-ray diffraction patterns of this phase consistently exhibit an fcc-based structure accompanied by a notable anomaly: the (200) diffraction peak appears at lower angles than predicted by lattice parameters derived from the (111) reflection. This behavior has prompted various interpretations, including deviations from cubic symmetry (e.g., tetragonal or monoclinic structures) [17,18]. However, synchrotron-based diffraction studies have not conclusively supported these non-cubic models [16]. Alternative explanations include the presence of multiple phases [1,3], the influence of stacking faults [16], or stress effects arising from pronounced elastic anisotropy [19]. More recently, high-resolution transmission electron microscopy investigations revealed a high density of stacking faults within the S-phase structure, although the anomalous (200) peak shift was attributed to a slightly distorted cubic symmetry, specifically a rhombohedral structure [20–23] or a tetragonal structure [24]. Despite over 40 years of research, the detailed crystal structure of the S-phase is still not fully understood.

Stainless-steel nitride thin films have attracted significant interest as protective and functional coatings due to their enhanced hardness, wear resistance, corrosion resistance, and thermal stability compared to untreated stainless steel [25–27]. However, the performance of stainless-steel nitride thin films is highly sensitive to deposition conditions, particularly substrate temperature, which strongly influences nitrogen incorporation, phase formation, microstructure, surface morphology, and mechanical behavior. Consequently, systematic optimization of substrate temperature is essential to achieve coatings with a favorable combination of high hardness, structural stability, and smooth surface morphology. Understanding and controlling these relationships is therefore critical for tailoring stainless-steel nitride thin films to specific application requirements.

Although stainless-steel nitride thin films have been widely investigated, most previous studies have primarily focused on phase identification or hardness enhancement under limited deposition conditions, often without establishing a comprehensive correlation between nitrogen incorporation, surface roughness, phase stability, and advanced mechanical performance indicators. In particular, the combined analysis of nitrogen content, surface morphology, and mechanical parameters such as H/E and H^3/E^2 over a broad substrate temperature range has received limited attention for sputtered stainless-steel nitride coatings. In the present study, nitrogen-containing stainless-steel thin films were deposited by reactive magnetron sputtering using an AISI 304 stainless-steel target. The primary objective is to systematically investigate the effect of substrate temperature (150–600 °C) on nitrogen incorporation and its influence on film composition, phase evolution, microstructure, surface roughness, and mechanical properties. The films were

characterized using X-ray photoelectron spectroscopy (XPS), X-ray diffraction (XRD), scanning electron microscopy (SEM), profilometry, and hardness measurements. By correlating deposition conditions with structural and mechanical responses, this work identifies an optimal growth regime and provides new insight into the deposition–structure–property relationships of stainless-steel nitride thin films relevant to wear-resistant and protective coating applications.

2. Materials and Methods

Synthesis. The stainless-steel nitride thin films were deposited using reactive magnetron sputtering in a high-vacuum chamber with a base pressure of approximately 1×10^{-6} Torr (1.3×10^{-4} Pa). A commercial AISI 304 stainless-steel target (18 wt.% Cr, 8 wt.% Ni, and 74 wt.% Fe) was used as the sputtering source. Deposition was performed in an Ar/N_2 gas mixture with flow rates of 20 sccm Ar and 5 sccm N_2, maintaining a working pressure of 0.67 Pa. A 50 mm diameter magnetron sputter gun powered by an RF power supply was employed. Prior to nitride deposition, a metallic stainless-steel bond layer was deposited using pure Ar with an applied substrate bias of −50 V to enhance adhesion. The bond layer thickness was approximately 60 nm. All nitride films were deposited at an RF power of 150 W. Film thickness was monitored in situ using a quartz crystal microbalance (INFICON Inc., East Syracuse, NY, USA). and subsequently verified by SEM cross-sectional analysis. Deposition times of 2 h were used, resulting in a typical growth rate of approximately 1 μm/h.

Characterizations. Structural characterization was performed using X-ray diffraction (XRD) with a Shimadzu XRD-6100 diffractometer (Shimadzu Scientific Instruments, Inc., Columbia, MD, USA) equipped with Cu Kα radiation (λ = 1.54 Å). Film composition was analyzed by X-ray photoelectron spectroscopy (XPS, Kratos Analytical Ltd., Manchester, UK) to determine elemental concentrations and calculate N/Me ratios. XPS measurements were conducted using a monochromatic Mg Kα source operating at 15 kV and 10 mA. Spectra were acquired over a binding energy range of 0–1200 eV with a dwell time of 200 ms, a step size of 1 eV, and a pass energy of 160 eV. Prior to analysis, surface contamination was removed by sputter etching with a 4 keV Ar^+ ion beam. Core-level spectra of Fe 2p, Cr 2p, Ni 2p, N 1s, and O 1s were analyzed. The average compositional deviation was ±1.5 at.%, with a standard deviation of ±1.1 at.%, from which the error range for the N/Me ratio was calculated. Film morphology was examined using cross-sectional SEM images obtained by fracturing Si substrates and analyzing the films with a Tescan Lyra FIB-SEM (TESCAN Group a.s., Brno, Czech Republic) operating at 6 keV. Surface roughness was quantified using a stylus profilometer to measure the arithmetic average roughness. For each sample, roughness measurements were performed at multiple locations across the film surface. Mechanical properties were evaluated by micro-indentation using a Knoop indenter under a load of 10 g. Hardness values were obtained from multiple indents for each sample to ensure statistical reliability.

3. Results and Discussion

3.1. Film Composition Analysis

X-ray photoelectron spectroscopy (XPS) was employed to investigate the chemical composition of stainless-steel nitride thin films deposited at different substrate temperatures. The measured concentrations of Fe, Cr, and Ni are summarized in Table 1. As expected, the elemental composition of all films closely matched the nominal composition of AISI 304 stainless steel. To confirm this, the Cr/Fe and Ni/Fe atomic ratios were calculated and are also presented in Table 1. The average Cr/Fe ratio was approximately 0.28, while the Ni/Fe ratio was around 0.11, both in good agreement with the nominal values

of 0.26 and 0.10, respectively, indicating that the sputtering process preserved the alloy composition across the investigated temperature range.

Table 1. Chemical composition and atomic ratios of the deposited coatings at different deposition temperatures.

Temp., °C	At.% Fe	At.% Cr	At.% Ni	At.% N	Cr/Fe	Ni/Fe	N/(Fe+Cr+Ni)
150	49.9	12	7.4	30.7	0.24	0.14	0.44
250	48.3	12.6	6.8	32.3	0.26	0.14	0.47
350	47.3	13	5.7	34	0.27	0.12	0.51
450	50.3	13.6	7.1	28.9	0.28	0.14	0.40
500	59.1	19.8	5.36	17.7	0.33	0.09	0.21
600	63.2	20.15	5.40	11.8	0.31	0.08	0.13

The nitrogen content was quantified as an absolute value and subsequently expressed as a nitrogen-to-metal ratio, where the metal content corresponds to the sum of Fe, Cr, and Ni. As shown in Table 1, the nitrogen content exhibits a pronounced dependence on substrate temperature. With increasing substrate temperature from 150 to 350 °C, the nitrogen content increases steadily and reaches a maximum value at 350 °C. This behavior is attributed to enhanced adatom mobility and increased nitrogen diffusion into interstitial sites of the face-centered cubic stainless-steel lattice at intermediate temperatures, which facilitates the formation of a nitrogen-supersaturated γN (S-phase).

At higher substrate temperatures, particularly above 450 °C, the nitrogen concentration decreases significantly with further increases in temperature. This reduction is associated with thermally activated nitrogen desorption from the film surface and enhanced diffusion of nitrogen out of the growing film, which reduces the effective nitrogen retention. In addition, the metastable γN phase becomes increasingly unstable at elevated temperatures, leading to its decomposition into equilibrium phases such as CrN, bcc-Fe, and fcc-Ni. These phase transformations further limit nitrogen incorporation by reducing the number of available interstitial sites for nitrogen accommodation.

Overall, the compositional analysis reveals a non-monotonic dependence of nitrogen incorporation on substrate temperature, with an optimum at 350 °C. This temperature represents a kinetic balance at which nitrogen diffusion into the growing film is maximized without significant nitrogen loss through desorption or phase decomposition, in good agreement with the observed structural and mechanical property evolution discussed in subsequent sections.

3.2. Crystal Structure

Figure 1 presents the X-ray diffraction (XRD) patterns of stainless-steel nitride thin films deposited on Si substrates at a substrate bias of −100 V, using an Ar/N_2 gas mixture of 20/5 sccm, with substrate temperatures ranging from 150 to 600 °C. Two distinct diffraction behaviors are observed depending on the deposition temperature. Films deposited at higher temperatures (500–600 °C) exhibit diffraction patterns that closely match those of CrN and bcc-Fe reference phases. In addition, the Ni (111) reflection at approximately 44.6° is nearly coincident with the bcc-Fe (110) peak at 44.7°, indicating that these films possess a multiphase structure consisting of CrN, bcc-Fe, and fcc-Ni. In contrast, films deposited at lower temperatures (150–350 °C) display diffraction patterns characteristic of a face-centered cubic (fcc) structure, with prominent (111), (200), (311), and (222) reflections within the scanned angular range. These patterns are consistent with the formation of a nitrogen-supersaturated austenitic phase (γ_N or S-phase). The reference γ_N diffraction pattern

was calculated using a lattice parameter determined from the position of the (111) peak. As the substrate temperature increases within this lower temperature regime, a gradual shift in the (200) reflection toward higher diffraction angles is observed, which correlates with a reduction in nitrogen content in the films. Approximate lattice parameters were estimated from the positions of the (111) and (200) reflections using Bragg's law, assuming a face-centered cubic structure. The calculated lattice constants show values in the range of 0.394–0.410 Å for films deposited between 150 and 350 °C, which are significantly larger than that of untreated austenitic stainless steel, confirming lattice expansion due to nitrogen supersaturation. Minor differences between lattice parameters derived from different reflections are attributed to residual stress, preferred orientation, and peak overlap effects. Since no full peak fitting or Rietveld refinement was performed, the extracted values are considered semi-quantitative and are used to support qualitative phase identification rather than detailed structural refinement. The diffraction pattern obtained at 450 °C exhibits feature of both regimes, suggesting a transitional microstructure between the nitrogen-supersaturated fcc phase and the multiphase structure observed at higher temperatures. This is a common observation for this phase [26–29].

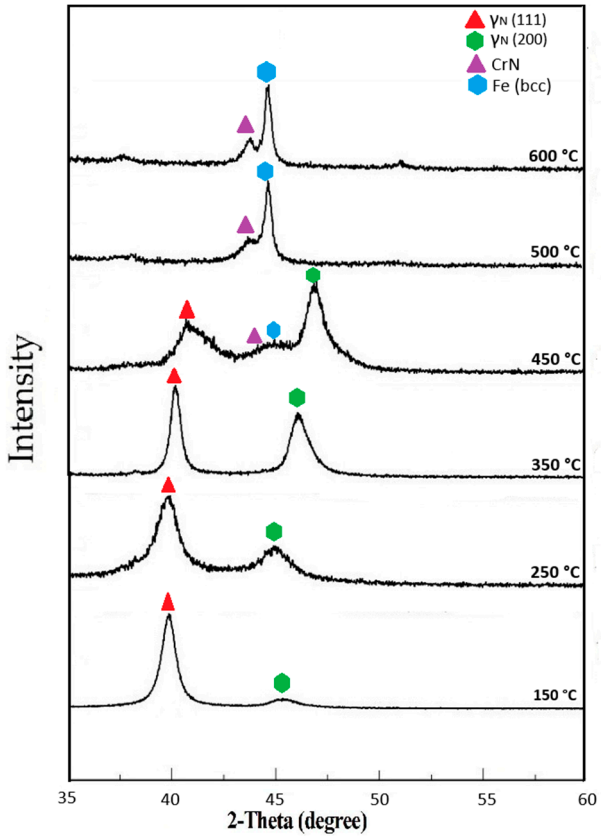


Figure 1. X-ray diffraction patterns of stainless-steel nitride thin films deposited at substrate temperatures from 150 to 600 °C. At low temperatures (150–350 °C), the films exhibit a nitrogen-supersaturated fcc γ_N (S-phase) structure with dominant γN (111) and γN (200) reflections. At higher temperatures (500–600 °C), additional peaks corresponding to CrN and bcc-Fe (110) phases appear, indicating a multiphase structure. The pattern at 450 °C shows features of both regimes, consistent with a transitional microstructure.

3.3. Film Morphology

SEM cross-section images of stainless-steel nitride thin films deposited at different substrate temperatures are presented in Figure 2. The film deposited at 150 °C exhibits a generally columnar structure with sharp, angular, and faceted grains. Small wedge-shaped

crystallites are observed, and the surface shows pronounced faceting on top of the columns. This morphology suggests a relatively porous film structure. At a substrate temperature of 250 °C, the film shows larger crystallites and voids, while the columnar structure becomes more continuous. A further increase in substrate temperature to 350 °C results in a more uniform and well-defined columnar structure, with less faceting compared to the films deposited at lower temperatures, leading to a smoother surface morphology. It is also noted that this film exhibits the highest nitrogen content in the present study (N/Me = 0.51). For the film deposited at 450 °C, a worm-like morphology is observed, although noticeable faceting remains. This structural change coincides with a phase transformation in the films, where a mixture of CrN, bcc-Fe, and fcc-Ni begins to form at this temperature. Films deposited at 500 and 600 °C exhibit a nodular or particle-like morphology, indicating microstructural coarsening due to enhanced grain growth at elevated substrate temperatures. This morphology is distinctly different from the fine columnar structures observed at lower deposition temperatures.

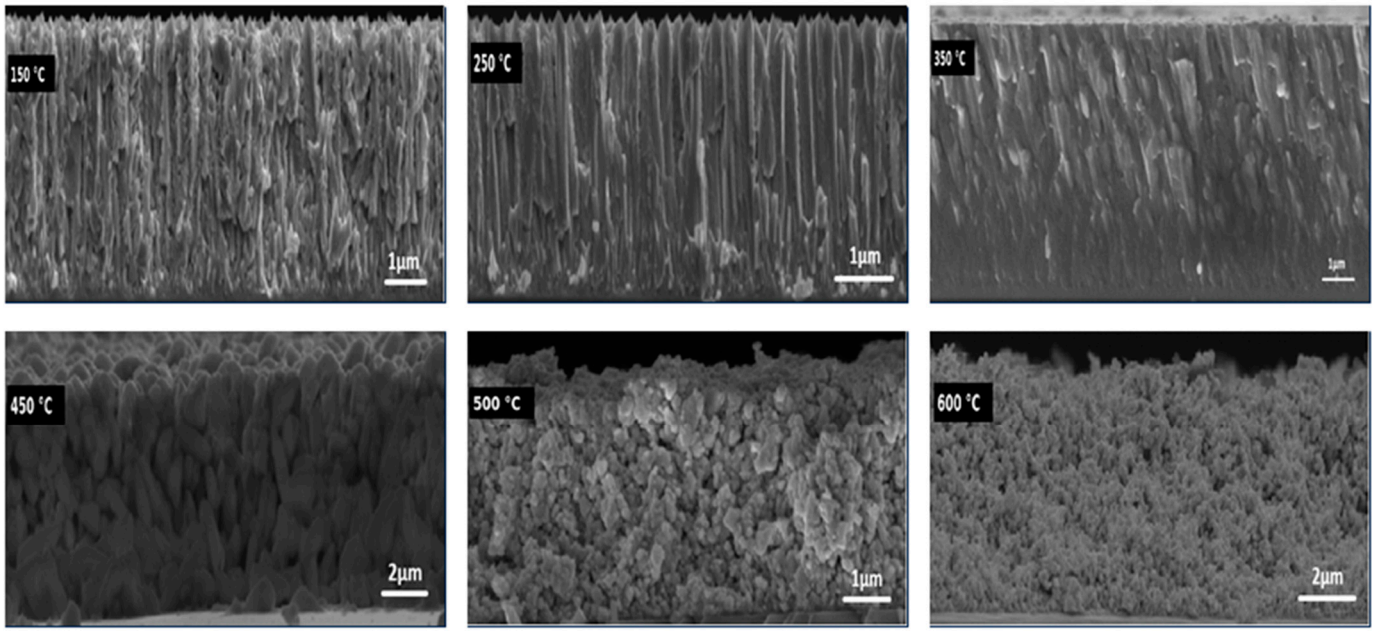


Figure 2. Cross-sections of stainless-steel nitride thin films deposited at different substrate temperatures (150–600 °C).

3.4. Surface Roughness

Figure 3 presents the variation in surface roughness (Ra), measured using a stylus profilometer, as a function of substrate temperature for the stainless-steel nitride thin films. As the substrate temperature increased from 150 to 350 °C, the surface roughness decreased from approximately 0.015 µm to a minimum value of about 0.006 µm. This reduction in roughness coincides with the increase in nitrogen content from 30 wt.% to 34 wt.%, as determined by XPS analysis. The decrease in roughness at intermediate substrate temperatures is consistent with the SEM observations across the investigated temperature range, which show a transition from faceted, porous columnar structures at lower temperatures to a more uniform and compact columnar morphology at 350 °C. At this temperature, enhanced adatom mobility and higher nitrogen incorporation promote grain coalescence and microstructural densification, resulting in a smoother film surface. At 350 °C, the balance between surface diffusion and nucleation density favors lateral grain growth rather than competitive columnar growth, suppressing the formation of surface asperities. This growth regime enables efficient filling of intercolumnar voids while limiting grain coarsen-

ing, thereby minimizing surface roughness. The formation of a nitrogen-supersaturated S-phase further contributes to the reduction in surface topographical irregularities [30–32]. At higher substrate temperatures (≥450 °C), the surface roughness increases again, reaching approximately 0.012 µm at 450 °C and further rising to 0.020–0.025 µm at 500–600 °C. This increase in roughness correlates with a decrease in nitrogen content due to thermally activated diffusion and desorption, as well as significant changes in film microstructure [33,34]. SEM images at these temperatures (450–600 °C) reveal the development of worm-like, nodular, and particle-like morphologies, which introduce larger surface features and increased roughness. The combined profilometry and SEM results indicate the existence of an optimal substrate temperature of 350 °C, where nitrogen incorporation is maximized and microstructural densification leads to the smoothest stainless-steel nitride thin films.

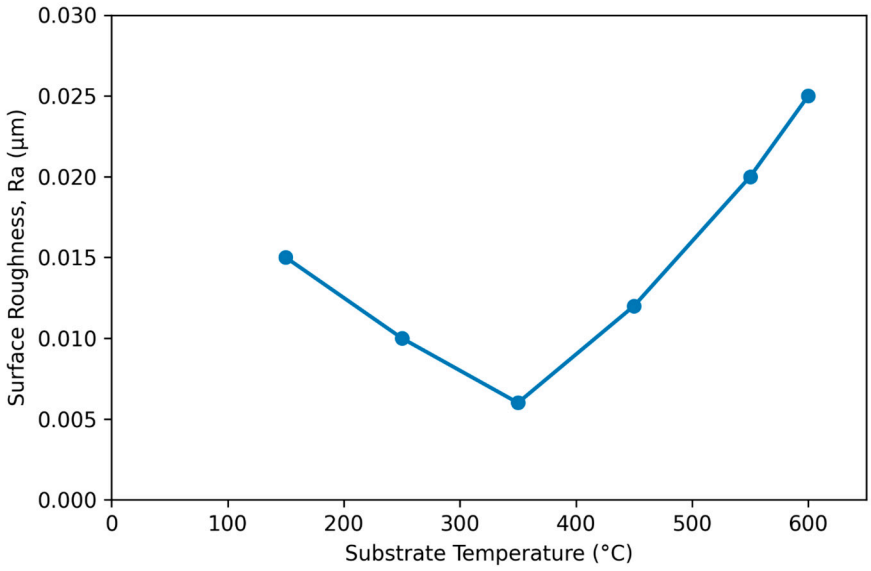


Figure 3. Variation in surface roughness (Ra) of stainless-steel nitride thin films as a function of substrate temperature. The roughness decreases with increasing temperature up to 350 °C, reaching a minimum value, and then increases at higher temperatures due to nitrogen loss and microstructural coarsening.

3.5. Mechanical Properties

The mechanical properties of the stainless-steel nitride thin films deposited at different substrate temperatures were evaluated using the micro-Knoop hardness method. Figure 4 shows the variation in hardness as a function of substrate temperature. The results clearly demonstrate that the hardness of the films is strongly dependent on substrate temperature. As the substrate temperature increased from 150 to 350 °C, the hardness increased steadily, reaching a maximum value of 1910 kgf/mm^2 at 350 °C, which is the highest hardness achieved in this study. The measured hardness is higher than values reported in earlier studies [2,35–37], which commonly reported hardness values between 1000 and 1450 HV. The enhanced hardness obtained in this study is primarily attributed to the highest nitrogen content (34 wt.%) measured by XPS at this temperature, which promotes the formation of a dense, nitrogen-supersaturated S-phase. SEM observations at 350 °C reveal a compact and well-defined columnar microstructure with reduced faceting and minimal porosity, which contributes to improved load-bearing capacity and mechanical strength.

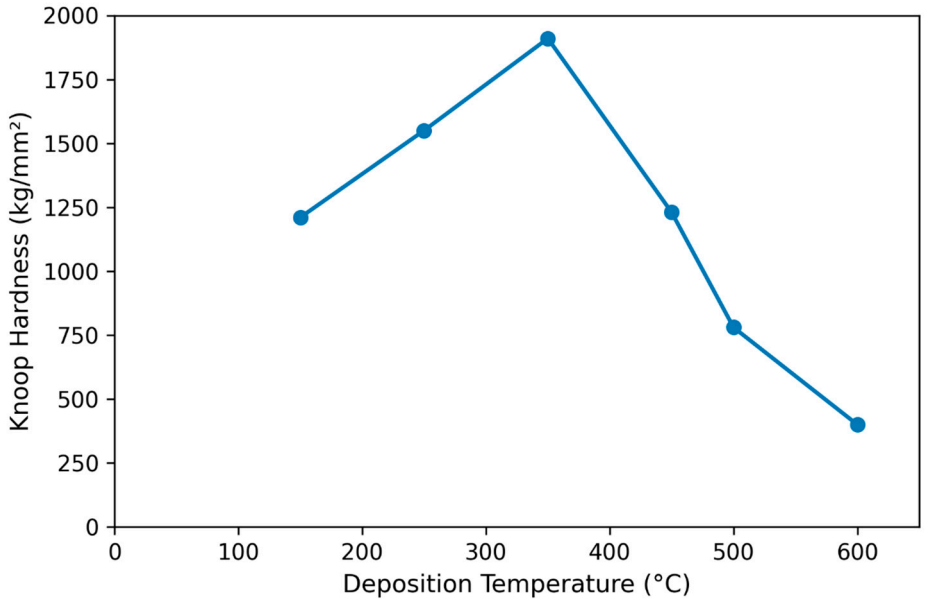


Figure 4. Variation in Knoop hardness as a function of deposition temperature. The hardness increases with temperature up to 350 °C and decreases significantly at higher temperatures.

In addition to hardness, the calculated H/E ratio (0.125) and H^3/E^2 ratio (30) also reach their maximum values at 350 °C. These parameters are widely used indicators of elastic strain tolerance and resistance to plastic deformation [38,39], respectively. The simultaneous increase in hardness, H/E, and H^3/E^2 at this temperature indicates that the film exhibits an optimal balance between high strength and elastic compliance, which is essential for accommodating applied stresses without premature failure. This enhanced mechanical performance is attributed to the maximum nitrogen incorporation at 350 °C, promoting the formation of a dense, nitrogen-supersaturated γN (S-phase) with a compact microstructure and minimal porosity. Furthermore, the surface roughness measured by stylus profilometry shows a minimum value of approximately 0.006 μm at 350 °C, reflecting the smooth and dense surface morphology observed in the SEM cross-sectional images. The combination of high hardness, favorable elastic and plastic deformation resistance, and low surface roughness is particularly beneficial for applications requiring reduced friction, improved load-bearing capacity, and enhanced wear resistance.

At higher substrate temperatures (450–600 °C), a noticeable degradation in mechanical performance is observed. The hardness, H/E ratio, and H^3/E^2 ratio decrease significantly with increasing temperature, correlating with a reduction in nitrogen content due to thermally activated nitrogen diffusion and desorption. In this temperature range, XRD results indicate a transition from the metastable γN phase to a mixture of equilibrium phases, including CrN, bcc-Fe (α-Fe), and fcc-Ni, which are less effective in providing solid-solution strengthening. SEM cross-sectional images further reveal pronounced microstructural changes, including grain coarsening and the development of worm-like, nodular, and particle-like morphologies associated with less compact growth. These microstructural changes lead to increased surface roughness, which rises to approximately 0.020–0.025 μm at 500–600 °C, further contributing to reduced hardness and mechanical reliability. The mechanical properties as a function of substrate temperature are summarized in Table 2, providing a comprehensive overview of the relationships among hardness, elastic strain tolerance, and resistance to plastic deformation. Based on these results, a substrate temperature of 350 °C is identified as the optimal deposition condition, yielding films with maximum hardness, superior resistance to elastic and plastic deformation, and the smoothest surface morphology. Compared with earlier reports on sputtered stainless-steel nitride

films, the present study achieves higher hardness together with lower surface roughness at comparable nitrogen contents, highlighting the effectiveness of substrate temperature optimization at 350 °C.

Table 2. Mechanical properties of stainless-steel nitride thin films deposited at different substrate temperatures. The Young's modulus (E) was not measured independently; instead, effective E values were derived from the measured hardness and H/E ratios and used for comparative analysis of mechanical performance.

Substrate Temperature (°C)	Nitrogen Content (wt.%)	Hardness (kgf/mm^2)	H/E	H^3/E^2	Surface Roughness (μm)
150	30	1210	0.079	8.1	0.015
250	32	1550	0.101	16.9	0.010
350	34	1910	0.125	30.0	0.006
450	29	1230	0.081	8.5	0.012
500	17	780	0.051	2.2	0.020
600	15	400	0.026	0.3	0.025

Based on the combined compositional, structural, morphological, and mechanical analyses, a substrate temperature of 350 °C provides the optimal combination of properties for wear-resistant and protective coating applications. At this temperature, XPS results reveal the highest nitrogen incorporation (34 wt.%), which promotes the formation of a stable nitrogen-supersaturated γN (S-phase) as confirmed by XRD. SEM cross-sectional observations show a dense and compact microstructure with reduced porosity, while profilometry measurements indicate the minimum surface roughness (~0.006 μm). These structural features directly translate into superior mechanical performance, including maximum hardness (1910 kgf/mm^2), the highest H/E ratio, and the highest H^3/E^2 ratio, indicating enhanced resistance to elastic and plastic deformation. At lower substrate temperatures, insufficient adatom mobility limits densification and nitrogen uptake, whereas at higher temperatures nitrogen loss, phase decomposition, and microstructural coarsening degrade both surface quality and mechanical reliability. Therefore, 350 °C represents an optimal growth regime where deposition kinetics, phase stability, and mechanical performance are simultaneously optimized.

4. Conclusions

A systematic study of stainless-steel nitride thin films deposited by reactive magnetron sputtering at substrate temperatures between 150 and 600 °C reveals a strong correlation between deposition temperature, nitrogen incorporation, microstructure, surface morphology, and mechanical properties. XPS results show that the nitrogen content increases with substrate temperature, reaching a maximum value of 34 wt.% at 350 °C, before decreasing at higher temperatures due to thermally activated nitrogen diffusion and desorption. Surface roughness measurements indicate a minimum value of approximately 0.006 μm at 350 °C, which is associated with the formation of a dense, nitrogen-supersaturated S-phase, as confirmed by XRD and SEM analyses. Films deposited at this temperature exhibit a compact microstructure with reduced porosity and improved surface smoothness. Mechanical testing further demonstrates that the film deposited at 350 °C achieves the highest hardness (1910 kgf/mm^2) along with optimal H/E and H^3/E^2 ratios, indicating enhanced resistance to elastic and plastic deformation. In contrast, films deposited at higher substrate temperatures show reduced nitrogen content, microstructural coarsening, increased surface

roughness, and degraded mechanical performance, highlighting 350 °C as the optimal deposition temperature for wear-resistant applications.

Funding: This research received no external funding.

Data Availability Statement: Data are contained within the article.

Acknowledgments: The Researchers would like to thank the Deanship of Graduate Studies and Scientific Research at Qassim University for financial support (QU-APC-2026). We used an AI-based translation tool (ChatGPT-5.1, Open AI) to assist with language polishing. All scientific content and interpretations were verified and edited by the author.

Conflicts of Interest: The author declares no conflicts of interest.

References

1. Ozturk, O.; Williamson, D.L. Phase and composition depth distribution analyses of low-energy, high-flux nitrogen implanted stainless steel. *J. Appl. Phys.* **1995**, *77*, 3839–3847. [CrossRef]
2. Menthe, E.; Rie, K.-T.; Schultze, J.W.; Simson, S. Structure and properties of plasma-nitrided stainless steel. *Surf. Coat. Technol.* **1995**, *74–75*, 412–416. [CrossRef]
3. Liu, C.; Xu, F.; Suo, Z.; Li, C.; Gu, J. The Role of Nitrogen to Hydrogen Ratio in Evolution of γN Phase and Surface Properties of Plasma-Nitrided 316L Stainless Steel Bipolar Plate. *J. Mater. Eng. Perform.* **2025**, 1–8. [CrossRef]
4. Alresheedi, F. Comparative Study of Nanocrystalline Dysprosium Oxide Thin Films Deposited on Quartz Glass and Sapphire Substrates by Means of Electron Beam. *Nanomaterials* **2025**, *16*, 10. [CrossRef]
5. Alresheedi, F. Superior resistive switching performance in SnO_2 nanoparticles embedded TiO_2 nanorods-based thin films. *Ceram. Int.* **2023**, *49*, 19505–19512. [CrossRef]
6. Galdikas, A.; Andriūnas, P.; Czerwiec, T.; Marcos, G.; Moskaliovienė, T. Modeling of Plasma Nitriding and Thermal Annealing Processes of Austenitic Stainless Steel. *Phys. B Condens. Matter* **2025**, *714*, 417487. [CrossRef]
7. Moher, D.; Shanahan, R.; Thimsen, E. Stabilization of III-nitrides at high temperatures using nitrogen plasma. *Appl. Phys. Lett.* **2025**, *126*, 151903. [CrossRef]
8. Richter, E.; Günzel, R.; Parascandola, S.; Telbizova, T.; Kruse, O.; Möller, W. Nitriding of stainless steel and aluminum alloys by plasma immersion ion implantation. *Surf. Coat. Technol.* **2000**, *128*, 21–28. [CrossRef]
9. Saker, A.; Leroy, C.; Michel, H.; Frantz, C. Properties of sputtered stainless steel coatings and structural analogy with low-temperature plasma-nitrided layers of austenitic steels. *Mater. Sci. Eng. A* **1991**, *140*, 702–706. [CrossRef]
10. Bechir, M.B.; Alresheedi, F. Exploring photoconduction mechanisms in Lead-Free $Cs_3Sb_2I_9$ single crystal thin films. *Opt. Mater.* **2024**, *157*, 116053. [CrossRef]
11. Kappaganthu, S.R.; Sun, Y. Formation of an MN-type cubic nitride phase in reactively sputtered stainless steel–nitrogen films. *J. Cryst. Growth* **2004**, *267*, 385–393. [CrossRef]
12. Kappaganthu, S.R.; Sun, Y. Influence of sputter deposition conditions on phase evolution in nitrogen-doped stainless steel films. *Surf. Coat. Technol.* **2005**, *198*, 59–64. [CrossRef]
13. Borowski, T.; Wójcik, H.; Spychalski, M.; Adamczyk-Cieślak, B. Wear and Corrosion Resistance of Thermally Formed Decorative Oxide Layers on Austenitic Steel. *Metals* **2025**, *15*, 707. [CrossRef]
14. Liu, C.; Zhang, F.; Zhang, L.; Peng, J.; Chang, H.; Wang, Y. Innovative Short Process of Preparation and Nitriding of Porous 316L Stainless Steel. *Materials* **2025**, *18*, 1564. [CrossRef] [PubMed]
15. Baranowska, J.; Fryska, S.; Suszko, T. Influence of temperature and nitrogen pressure on S-phase coatings deposited by reactive magnetron sputtering. *Vacuum* **2013**, *90*, 160–166. [CrossRef]
16. Fewell, M.P.; Mitchell, D.R.G.; Priest, J.M.; Short, K.T.; Collings, G.A. The nature of expanded austenite. *Surf. Coat. Technol.* **2000**, *131*, 300–306. [CrossRef]
17. Liu, Z.; Han, C.; Cao, X.; Guo, J.; Li, H.; Lin, Y.; Yang, J.; Liu, W. Microstructure and wear behavior of AISI 316L austenitic stainless steel coating fabricated by laser cladding and plasma nitriding. *Mater. Lett.* **2025**, *383*, 137951. [CrossRef]
18. Shen, L.; Wang, W.; Zhao, W.; Hui, Z.; Sui, J.; Sun, P. The structure evolution of austenite stainless steel with pre-shot peening during plasma nitriding. *J. Phys. Conf. Ser.* **2024**, *2775*, 012030. [CrossRef]
19. Mändl, S.; Rauschenbach, B. Anisotropic strain in nitride austenitic stainless steel. *J. Appl. Phys.* **2000**, *88*, 3323–3329. [CrossRef]
20. Stroż, D.; Psoda, M. TEM studies of plasma-nitrided stainless steel. *J. Microsc.* **2010**, *237*, 227–234. [CrossRef]
21. Selvabharathi, R.; Rajarajan, P.C.; Kulathuraan, K. Influence of Ni alloy content on Ni–$BiFeO_3$ crystal phase and tribology of laser claddings. *Int. J. Precis. Eng. Manuf.* **2025**, *26*, 2929–2945. [CrossRef]

22. Xia, J.; Zhang, J.; Huang, K.; Zhang, B.; Wu, F.; Liang, Y.; Wu, J. In situ growth of an active catalytic layer on stainless steel for oxygen evolution reaction. *J. Mater. Chem. A* **2024**, *12*, 19008–19017. [CrossRef]
23. Alresheedi, F. Structure and spectroscopic ellipsometry studies of nanocrystalline Dy_2O_3 thin films deposited on Al_2O_3 wafers by electron beam evaporation technique. *J. Mater. Res. Technol.* **2021**, *12*, 2104–2113. [CrossRef]
24. Fewell, M.P.; Priest, J.M. Higher-order diffractometry of expanded austenite using synchrotron radiation. *Surf. Coat. Technol.* **2008**, *202*, 4208–4212. [CrossRef]
25. Yadav, A.; Srivastava, M.; Jain, P.K.; Rathee, S. Microstructure transformations and improving wear resistance of austenitic stainless steel additively fabricated by arc-based DED process. *Def. Technol.* **2024**, *38*, 194–204. [CrossRef]
26. Borgioli, F. Expanded phases in low-temperature treated stainless steels: A review. *Metals* **2022**, *12*, 331. [CrossRef]
27. Gumuslu, T.; Kaba, M.; Atar, E.; Cimenoglu, H. Effect of low-temperature nitriding on wear behavior of austenitic stainless steel. *Tribol. Int.* **2023**, *185*, 108560. [CrossRef]
28. Tang, D.; Zhang, C.; Zhan, H.; Huang, W.; Ding, Z.; Chen, D.; Cui, G. High-efficient gas nitridation of AISI 316L stainless steel. *Coatings* **2023**, *13*, 1708. [CrossRef]
29. Zhang, X.; Liu, Y.; Ma, Z.; Chen, S.; Ma, M.; Yang, D.; Wu, Z. Integrated nitriding and DLC deposition on 316L stainless steel. *Surf. Coat. Technol.* **2025**, *496*, 131716.
30. Anders, A. A structure zone diagram including plasma-based deposition and ion etching. *Thin Solid Film.* **2010**, *518*, 4087–4090.
31. Musil, J. Hard and superhard nanocomposite coatings. *Surf. Coat. Technol.* **2000**, *125*, 322–330. [CrossRef]
32. Lin, J.; Moore, J.J.; Mishra, B.; Pinkas, M.; Sproul, W.D.; Rees, J.A. Effect of asynchronous pulsing parameters on CrAlN films. *Surf. Coat. Technol.* **2008**, *202*, 1418–1436. [CrossRef]
33. Larisch, B.; Brusky, U.; Spies, H.J. Plasma nitriding of stainless steels at low temperatures. *Surf. Coat. Technol.* **1999**, *116*, 205–211. [CrossRef]
34. Khoshman, J.M.; Peica, N.; Thomsen, C.; Maultzsch, J.; Bastek, B.; Wan, C.; Kordesch, M.E. Growth and surface characterization of magnetron sputtered zinc nitride thin films. *Thin Solid Film.* **2012**, *520*, 7230–7235. [CrossRef]
35. Adachi, S.; Yamaguchi, T.; Ueda, N. Formation and properties of nitrocarburizing S-phase on AISI 316L stainless steel. *Metals* **2021**, *11*, 1538. [CrossRef]
36. Fossati, A.; Borgioli, F.; Galvanetto, E.; Bacci, T. Glow-discharge nitriding of AISI 316L austenitic stainless steel. *Surf. Coat. Technol.* **2006**, *200*, 3511–3517. [CrossRef]
37. Sun, Y.; Li, X.; Bell, T. Low-temperature plasma carburising of austenitic stainless steels. *Surf. Eng.* **1999**, *15*, 49–54. [CrossRef]
38. Hu, H.; Guo, X.; Zhang, Y.; Chen, Z.; Wang, L.; Gao, Y.; Zheng, Z. Elasto-plastic design of ultrathin interlayers for flexible electronics. *ACS Nano* **2023**, *17*, 3921–3930. [CrossRef]
39. Fujii, T.; Kawarabayashi, K.; Shimamura, Y. Intergranular corrosion in sensitized austenitic stainless steel under elastic–plastic loading. *Corros. Sci.* **2024**, *230*, 111896. [CrossRef]

Disclaimer/Publisher's Note: The statements, opinions and data contained in all publications are solely those of the individual author(s) and contributor(s) and not of MDPI and/or the editor(s). MDPI and/or the editor(s) disclaim responsibility for any injury to people or property resulting from any ideas, methods, instructions or products referred to in the content.